

# Turing Pattern Formation from Reaction-Diffusion Equations and Applications

Physics 569 Term Essay

Riley Vesto

**Abstract:** Turing patterns are finite-wavelength, stationary formations which can develop from homogeneous initial conditions following local reaction-diffusion equations. This essay provides a phenomenological description of how Turing patterns form, describes methods of preparing Turing patterns, and provides some examples of Turing patterns which appear in nature.

May 2021

# 1 Introduction

Pattern formation is a phenomena seen throughout nature, where an initially homogeneous system evolves to form structures with one or more wavelengths, often in steady state. Examples range from reasonably recognizable patterns such as stripes or spots on animals to more abstract patterns like the branching patterns of leaves. A particular class of these patterns, known as Turing patterns, are steady-state solutions with wavelengths observed to be independent of the volume of space they occupy or boundary conditions, indicating that they are emergent from the interactions of microscopic degrees of freedom in the system.

Alan Turing formulated the formation of Turing patterns through the diffusion and reaction of morphogens which are typically species of chemicals or biological agents but can be as abstract as full organisms in predator-prey systems [1]. The dynamics of the concentration of these morphogens,  $X_i$ , are dictated by the diffusion-reaction equations:

$$\frac{\partial X_i}{\partial t} = g_i(X_1, \dots, X_n) + D_i \nabla^2 X_i \quad (1)$$

Where  $g_i$  are local functions of the full set of  $n$  morphogen concentrations and  $D_i$  is the diffusion coefficient for the  $i$ -th morphogen. The key feature of these equations is that the interactions are fully local, not depending on any spatial derivatives of  $X_i$ , and therefore Turing pattern formation is the result of an emergent spatial scale from the consecutive reactions then diffusion of morphogens.

This paper seeks to explain how Turing patterns form phenomenologically, understand what the requirements for Turing pattern formation are, and how these requirements are interpreted in some examples of engineered or natural Turing patterns. We begin with the phenomenological description, using linear-stability analysis of the framework then discuss some of the implications and applications of Turing patterns in nature, using the Hydra as an example. Then we discuss a couple concrete and measured examples of Turing patterns, the chlorite-iodide malonic acid system and the stripe formation on zebra fish. Finally, we introduce how the set of Turing pattern examples might be expanded using stochastic rather than deterministic models.

## 2 Phenomenology

Turing patterns in reaction-diffusion systems are described as stationary, finite-wavelength solutions which arise from homogeneous initial conditions. Although not exactly necessary, these patterns generally arise from systems with two morphogens, an inhibitor and an activator whose local densities we write as  $X$  and  $Y$  respectively. We will apply linear stability analysis to build a description of such systems. Considering  $X$  and  $Y$  as small deviations away from equilibrium values, we can write the linearised reaction

diffusion equations:

$$\frac{\partial X}{\partial t} = -aX + bY + D_x \nabla^2 X \quad (2)$$

$$\frac{\partial Y}{\partial t} = -cX + dY + D_y \nabla^2 Y \quad (3)$$

where  $a, b, c, d$  are positive reaction rates and  $D_x$  and  $D_y$  are respective diffusion rates.

The idea behind pattern formation is that the inhibitor is able to diffuse fast enough to suppress the homogeneous growth of the activator. For example, we consider the activator as a prey, which reproduces and feeds predators, and the inhibitor as a predator, which feeds on the prey and is territorial as to scare away other predators. If the predator is too slow, then the prey overgrows and forms a homogeneous final state. However, if the predator is sufficiently fast then the predator is able to herd the prey into stationary territories of prey where it feeds. That is assuming the feeding rate of the predator is sufficiently small as to not overfeed and kill off the prey. This suggests a condition with  $D_x > D_y$  for the formation of Turing patterns [11].

Asserting a solution of the form  $X \propto Y \propto e^{ikx + \omega t}$ , then dispersion relationship is provided as the solution to the eigenvalue equation:

$$\omega_{\pm}(k) = \frac{d-a}{2} - \frac{D_x + D_y}{2} k^2 \pm \sqrt{\left(\frac{d+a}{2} + \frac{D_x - D_y}{2} k^2\right)^2 - bc}. \quad (4)$$

If we assume a uniform initial condition with deviation away from equilibrium concentrations  $X = Y = 0$ , then the formation of patterns requires some instability which can be achieved if  $\text{Re}(\omega_{\pm}(k)) > 0$  at some wavelength, in which case the Fourier components of the densities at said  $k$  will grow exponentially towards some other fixed-point. To describe these fixed-points we will need a full picture of the non-linear reaction rates, outside of this linear stability analysis.

Nonetheless, the linear stability procedure follows. If  $\text{Re}(\max_k \omega_{\pm}(k)) > 0$  then the system will evolve to a new equilibrium and if  $\arg \max_k \omega_{\pm}(k) \neq 0$  or  $\infty$  then the new equilibrium will consist of some wavelength which forms our Turing pattern. As such we work only with  $\omega_+$  which automatically satisfies this condition for  $\omega_-$ . The finite wavelength critical point is:

$$k_0 = \frac{1}{D_x - D_y} \left[ (D_x + D_y) \sqrt{\frac{bc}{D_x D_y}} - (a + d) \right], \quad (5)$$

with:

$$\omega_+(k_0) = \frac{1}{D_x - D_y} \left( aD_x + dD_y - 2\sqrt{bcD_x D_y} \right). \quad (6)$$

The conditions for  $\omega(k_0) > \omega(0) = (d-a)/2 + \sqrt{(d+a)^2/4 - bc}$  and  $\omega(k_0) > 0$  is then [1]:

$$\frac{4\sqrt{D_x D_y}}{D_x + D_y} < \frac{a+d}{\sqrt{bc}} < \frac{D_x + D_y}{\sqrt{D_x D_y}} \quad (7)$$

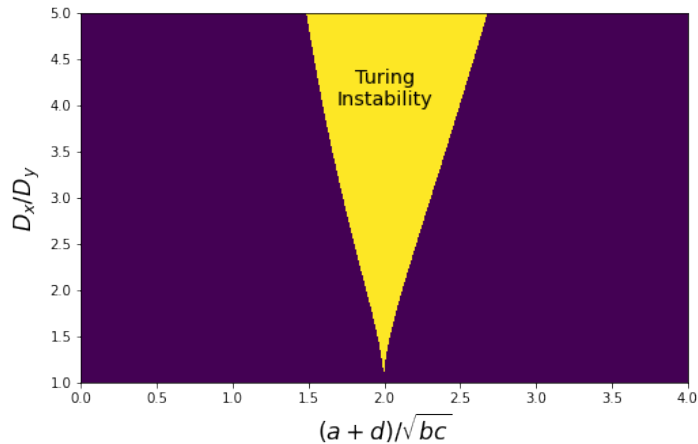


Figure 1: Phase diagram for the onset of Turing instabilities in the linearised model system.

A phase diagram of this condition is provided in Fig. 1 and the result is that for  $(a + d)/\sqrt{bc} = 2$ , then any  $D_x/D_y$  admits Turing patterns, since the corresponding reaction rates are well balanced. Otherwise, we generally need that  $D_x \gg D_y$  which was our expected result.

### 3 Implications

Throughout this process, we've made no mention of boundary conditions and fundamentally, we don't need to. This is because Turing patterns arise as an emergent scale from the local interactions in the system. If we had introduced boundary conditions, periodic for instance, then the continuum of admissible wavelengths would be discretized. However, the system would still be able to evolve towards a wavelength nearby  $k_0$ .

Further, our analysis can be interpreted as a form of spontaneous breaking of parity symmetry. The linearised reaction-diffusion equations are symmetric under reflections,  $x \mapsto -x$ , which generally is a property of simple systems. However, once the Turing instability forms, a bifurcation develops with new steady-states at  $k = \pm k_0$ . Therefore, the parity symmetry has to break and the system effectively chooses a handedness by which finite-wavelength fixed point it evolves to.

Turing originally proposed that this method of pattern formation could be used to account for various asymmetries observed in biology such as the branching patterns seen in leaves or left-/right-handedness in organisms [1]. As a specific example, Turing proposes the Hydra which is a small (not quite micro-) freshwater organism consisting of a tube (body) with 4-6 tentacles extruding from one end (the head). Being a relatively simple organism, it would seem counter-intuitive that the developing hydra can seemingly break the radial symmetry of its body to form the asymmetric tentacles

of its head.

Hydra, in fact, show some more breaking of asymmetry which ultimately turn out to be related to reaction-diffusion processes. Hydra reproduce asexually by budding, which already requires pattern formation, and if cut, may regenerate into two new hydra each with only one head, i.e., the portion cut away from the head somehow knows that it needs to grow a head whereas the other somehow knows it does not. This "polarity" of hydra is an example of an emergent asymmetry [2].

The role of interactions and diffusion of activators and inhibitors is demonstrated in hydra grafting experiments. Here it is proposed that the formation of a head is caused by the excess activator morphogen and the head produces inhibitor to prevent the formation of a second head [3]. If the hydra's head is removed then rapidly grafted to the opposite end, then the inhibitor is able to diffuse back through the hydra and prevent the formation of a second head. However, if some time elapses (4-6 hr) before the hydra's head is re-grafted then the activator concentration is able to overgrow and the hydra is able to grow a second head even after the first is re-grafted.

Ultimately, this is not a precise example of the Turing instability but rather just a demonstration of how the activator/inhibitor dynamics may play a role in determining the placement of the hydra's head. However, in Fig. 2, we observe the formation of multiple hydra from a single spherically symmetric aggregate of cells. This could be explained directly using Turing's instability. The initially symmetric state has the inhibitor and activator homogeneously distributed but the inhibitor is able to diffuse rapidly and herd the activator into some finite wavelength spherical harmonic which depend only on the diffusion/reaction rates. The maxima of the spherical harmonic correspond to excess activator, which results in the formation of buds (b). Eventually these buds sprout into heads (c) and the infusion of inhibitor from these new heads quell the formation of any more heads and the newly formed organisms split apart [2].

This model of the formation of hydra from an aggregate of cells seems to have some spectacular analogues in more complicated systems. As a direct comparison, the human blastula seems to undergo a similar process in order to form the beginnings of a gastrointestinal system and eventually the fetus. Ultimately, Turing's instability seems to suggest that relatively simple systems can develop extreme complexity. However, in practice this is not so easy as the requirements on morphogen diffusions are difficult

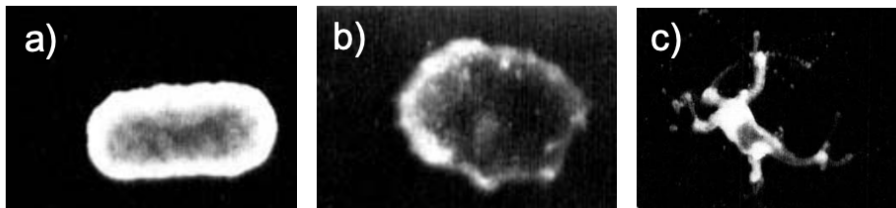


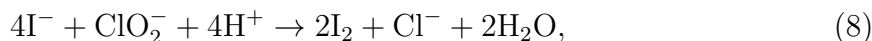
Figure 2: Formation of hydra from spherical aggregate of cells (a) by first forming asymmetric buds (b) then forming heads (c). Taken from [2].

to achieve.

### 3.1 Turing Patterns in Chemical Systems

Direct confirmation of Turing pattern formation required design of a chemical system which exhibited the inhibitor/activator structure. These systems are generally used for clock experiments where  $\omega$  takes on a complex part and the chemical concentrations exhibits oscillations. The most popular system is the Belousov-Zhabotinskii (BZ) reaction where bromate oxidizes an organic acid such as malonic acid [5]. However, this system has a narrow region in which Turing patterns can arise and a more controllable reaction was desired and the chlorite-iodide-malonic acid (CIMA) system was chosen [4].

The CIMA system consists of many reactions but the ones of predominant interest are:



where chlorite ( $\text{ClO}_2$ ) can be identified as the inhibitor for iodide ( $\text{I}^-$ ) and iodide undergoes redox with the neutral chlorine dioxide to activate chlorite [6]. The malonic acid (MA) acts as a reducing agent, to replenish iodide from elemental iodine or other oxidation states. The other reactions, such as oxidation of chlorite or iodide are considered to be controlled and negligible by the selection of malonic acid concentration [4]. All other species besides iodide and chlorite are assumed to be plentiful such that they do not deviate from equilibrium. This lends the following processes, with  $[X]$  representing the concentration of the reactant  $X$ ,  $X$  for iodide and  $Y$  for chlorite, the over-text on the arrows representing the reaction rate, and all other constants as chemical dependent quantities:



If we compile all constant reaction rates into unspecified constants, we can read off the reaction-diffusion equations:

$$\frac{\partial X}{\partial t} = a - bX - \frac{4cXY}{1 + X^2} + D_x \nabla^2 X \quad (13)$$

$$\frac{\partial Y}{\partial t} = bX - \frac{cXY}{1 + X^2} + D_y \nabla^2 Y \quad (14)$$

Then linearised about the homogeneous steady state ( $X_0 = a/(b + 4bc)$  and  $Y_0 = b(1 + X_0^2)$ ), we obtain a form similar to equation 2 to which some constraints need to be made for the reaction rates to ensure that iodide properly behaves as an activator.

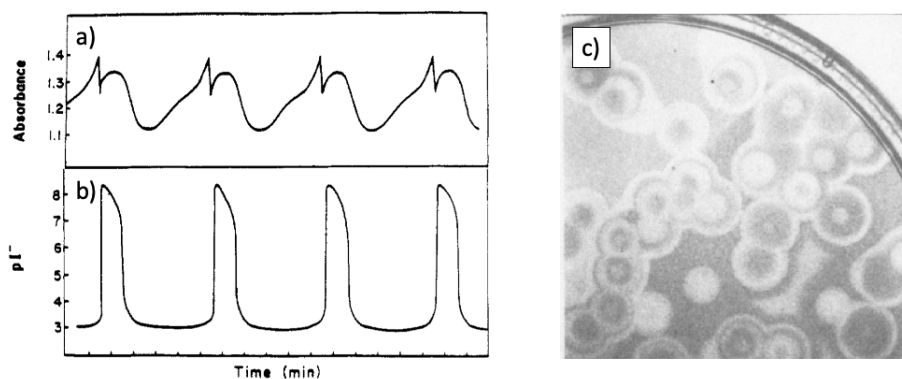


Figure 3: Demonstration of oscillatory behavior of iodide in CIMA system by 460 nm optical absorption (a) and iodide sensitive electrode. Wave-trigger pattern produced by propagation oscillation of iodide in Petri dish (c). Taken from [5].

Nonetheless, the CIMA system demonstrates an inhibitor/activator structure and therefore should show some semblance of pattern formation. Even better, iodide has a distinct yellow-ish tint, allowing patterns to be observed by eye or by measuring absorbance at 460 nm. Fig. 3a-b, demonstrates this through oscillations in the iodide concentration and absorbance and by adjusting the geometry of the setup, these oscillations can be made to propagate across a Petri dish, forming ring patterns as seen in Fig. 3c. However, these patterns are not Turing patterns. For one, the oscillatory nature means that they will rarely reach a patterned steady-state. But even if the oscillations are able to form standing waves, these waves will be defined by how long the oscillation takes to cross the dish and, therefore, will scale with the geometry of the setup [5].

In fact, the oscillations shown in Fig. 3a-b cannot be simply explained using our linearised model. The sharp transition between low and high iodide concentration in Fig. 3b indicates bistability of two equilibrium iodide concentration between which the whole system forms a limit cycle. This can also be used to explain the double peak in the absorbance, Fig. 3a, using hysteresis, where the iodide shows higher absorbance on approach to the high concentration fixed point. This hysteresis is confirmed by direct measurement [5].

So the CIMA system alone doesn't show Turing patterns and our previous analysis explains why. Generally speaking, the diffusion coefficients of chemicals in aqueous solutions range from  $1-3 \times 10^{-5} \text{ cm}^2/\text{s}$  and if the chemical reactions are not well balanced, which is usually the case, then we'd require the inhibitor to diffuse at least 20-30 times as fast as the activator [4]. This simply is not possible for small molecules and, therefore, some modification is required.

Eventually Turing patterns were observed in the CIMA system once the reactions were carried out in a polyacrylamide gel reactor [4]. In this case, the iodide binds to

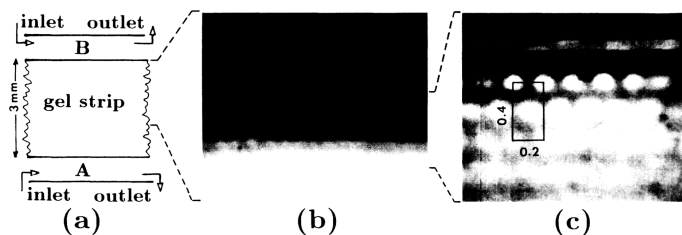


Figure 4: Demonstration of Turing pattern by CIMA system in a gel-reactor. Diagram of gel-reactor (a), large scale image of gel-strip after steady-state is achieved (b), small scale image of Turing pattern with 0.2 and 0.4 mm labeled (c). Taken from [4]

some added starch (S) through a reversible reaction:



This starch was actually already present as a dye in the petri-dish in Fig. 3c, however, the polyacrylamide gel slows down the reaction such that the iodide remains bound to the starch for a non-negligible time. The starch is bulky and particularly in the gel has an extremely low diffusion constant, therefore the chlorate is able to travel across the gel-strip much faster than the iodide.

Seen in Fig. 4c, the color in the gel forms colored dots, associated with high concentration of iodide, which are reminiscent of the solution  $X \sim e^{i2\pi x/\lambda} + e^{i2\pi y/\lambda}$ , where  $\lambda \approx 0.2$  mm. The isotropicity of the dots, despite non-isotropicity of the gel-strip ( $20 \times 3$  mm<sup>2</sup>) is indicative of Turing patterns. Furthermore, changing of the dimensions or disturbing the pattern results in the development of the same dimension. Instead, the wavelength is strongly dependent on temperature which suggests that it is determined by the reaction and diffusion rates alone, a signature of Turing patterns. Although the diffusion rates cannot be precisely controlled in order to determine the phase-boundary and dynamics near the transition between inhomogeneous state and instability, the malonic acid concentration can be used to tune the generation of iodide. The patterns are observed over a range of  $[MA] = 8-13$  mM, over which the wavelength does not vary by more than 20% [4].

These experiments seem to be discouraging for the hypothesis of Turing patterns being the driving force behind symmetry-breaking in the development of organisms. While diffusion of morphogens between cells is not necessarily constant, it seems pretty rare that a chemical inhibitor can achieve the excess speed required of pattern formation. In the following, we investigated some mechanisms by which Turing or Turing-like patterns might arise even when these conditions are not met.

## 4 Turing Patterns in Biological Systems

We've introduced the hydra as evidence that Turing patterns might be used to describe asymmetries in nature. However, this would require the inhibitor to diffuse much

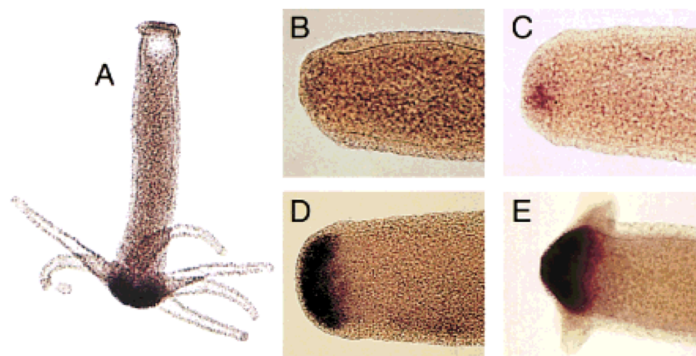


Figure 5: Micrographs of hydra with Hybra1 indicated in black. Before removal of the head, the Hybra1 is concentrated at the head (A). No Hybra1 is observed immediately after the head is removed (B), then the signal appears at 3 hr (B), is fully restored to original concentration at 4 hr (C), and begins to reform the head after 48 hr (C). Taken from [7]

faster than activator which seems inaccessible to conventional chemical systems such as aqueous solutions. However diffusion of morphogens between cells is much more varied.

In Turing's paper, he originally performed the analysis using a discrete model rather than the continuum described in section 2; his analogy being that the discrete points are cells with an internal equilibrium of morphogens but exchange morphogens intracellularly outside of equilibrium [1]. The analysis is the same as in section 2. However, the mechanism by which cells exchange morphogens may be more complicated than just diffusion. For example, if the cell wall is permeable to the inhibitor but mostly impermeable to the activator,  $X$ , then  $D_x \approx 0$  and the condition for Turing pattern formation is only dependent on the reaction rates. Additionally, activators and inhibitors inside cells may not interact strictly through reaction but by triggering or blocking receptors which controls the production of morphogens. This means that the morphogens are normally proteins which may be structurally varied with largely different diffusion rates [9].

An inhibitor signal or morphogen which can inhibit cells over a long range of cells, lateral inhibition, is well documented. For example, the human eye is able to distinguish sharp features when retina cells which receive light laterally inhibit adjacent cells, making them perceive less light and transforming what might otherwise be a slow gradient of light into a sharp feature [7]. Short-range activator signals or self-catalysis is somewhat less documented but tends to be easier to identify as its positive feedback loop results in the difference in concentration being much stronger on the pattern antinodes than for the inhibitor. For example, the proposed-activator HyBra1 gene is very concentrated on the head of a hydra, as seen in Fig. 5a, and when the head is removed, the signal reappears strongly before the new head grows, Fig. 5d-e [7].

For a more complicated example, the stripes on zebra fish (*Danio rerio*) demonstrate

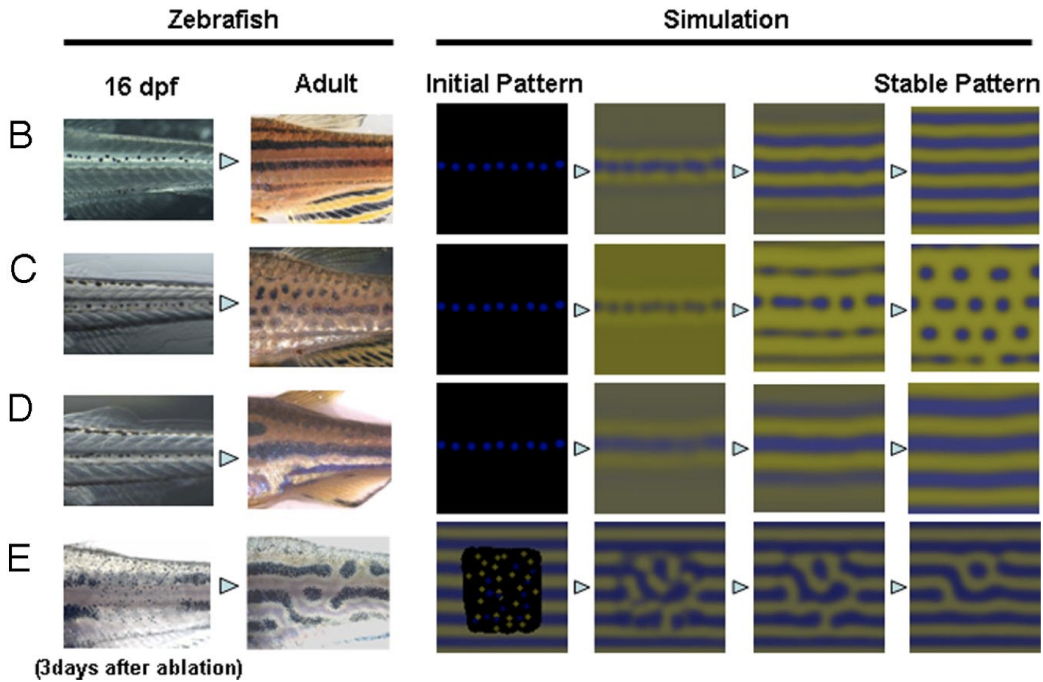


Figure 6: Demonstration of fit between reaction-diffusion model simulation and zebra fish spots. Patterns of adult zebra fish are predicted using 16 day-past-fertilization (16 dpf) patterns as initial conditions for the simulation, (B-D). The pattern of an adult zebra-fish’s stripes 3 days after laser ablation was additionally used to predict the stripes after fully regrown (E). Taken from [8]

behavior reminiscent of Turing patterns. These patterns are composed of multiple pigment containing cells but can be modeled as consisting of xanthophores (yellow) and melanophores (black). The local concentration of these cells determines the color within a certain region of the pattern [8].

Through a series laser ablation experiments, the interaction of adjacent cells were deduced. For example, if melanophores in a black stripe were destroyed by ablation then the xanthophores in an adjacent stripe would persist but if the experiment was reversed and xanthophores were destroyed in a yellow strip, then the melanophores in an adjacent stripe would die over time (10-15% reduction in 3 days). This indicated to the authors that the melanophores showed a long-range activation effect. The same process indicated that melanospheres had a long-range self-inhibition effect [8]. Shorter range effects were identified in younger zebra fish who had more randomly distributed pigment cells, allowing for ablation experiments to take place within strips. Ultimately it was deduced that both pigments had short-range inhibitory effects on each other [8].

The results of these experiments were fit to a 3-morphogen reaction-diffusion equation. Two morphogens were used to describe the xanthophores and melanophores concentrations, with small diffusion coefficients as the cells should not travel much. The third morphogen was described as a smaller, faster, unidentified molecule which

carried the long-range interactions. Because of the long-range self-inhibitory interaction of melanophores, this smaller molecule was determined to be an inhibitor in the network. The reaction rates were fit as linear coefficients but bounds were placed to ensure no non-physical fast reactions would occur [8].

As seen in Fig. 6b-d, the simulation was able to successfully predict the patterns on an adult Zebra fish using the patterns observed on the same zebra fish at 16 days post-fertilization. These included not only lateral stripes, but also equally spaced dots, demonstrating the richness of the patterns produced by such a nearly-linear network. Additionally, the simulation was able to accurately predict the patterns which reformed after some cells were ablated, Fig. 6e. These reformed patterns were particularly complex, demonstrating almost topological features. While these experiments do not directly demonstrate that the patterns are not dependent on boundary conditions, size of fish, the accuracy of the simulations confirm that the stripes can be and are likely formed by the relatively simple interactions captured in Turing’s model [8].

## 5 Stochastic Turing Patterns

We’ve seen that Turing patterns can arise in macroscopic or biological systems where morphogens of very different sizes interact to achieve the correct conditions for instability. Additionally, we’ve seen that Turing patterns can be formed in chemical systems with proper design. However, the formulation presented fails to describe the vast number of postulated examples of Turing pattern formation in nature. For example, cell division in simple cells would require inhibition and activation to be mitigated by small molecules which would have similar diffusion constants [7]. Therefore, we would require a modification to the current description.

One possible modification is the introduction of noisy forces to the concentrations in the reaction-diffusion equations:

$$\frac{\partial X_i}{\partial t} = g(X_1, \dots, X_N) + D_i \nabla^2 x_i + \xi_i(t)$$

where  $\xi_i(t)$  is mean-zero white noise:  $\langle \xi_i(t) \rangle = 0$  and  $\langle \xi_i(t) \xi_j(t') \rangle = B_{ij} \delta(t - t')$ . The transition between the previous deterministic reaction-diffusion models to this stochastic model is in effect identical to the shift between mean-field theory and higher orders in thermodynamic limit expansions of a statistical field theory, i.e., the introduction of this term and presumption that it has an effect requires that the thermal or concentration fluctuations are comparable to the system size. This might initially seem unjustified, since the systems which display Turing patterns are usually large compared to noise. However, the non-orthogonality of the eigenvectors for  $A_{ij}$  can result in extreme sensitivity to the noise through a process known as giant amplification [11].

Giant amplification and the field-theoretic techniques to analyze this stochastic reaction-diffusion system are outside the scope of this paper. However, once the power spectrum for the Fourier modes are determined, the Turing pattern formation can be

predicted just as in the linear stability analysis in section 2, by analyzing the conditions under which the amplification is largest for finite wavelength. Analysis of the Levin-Segel model for plankton-herbivore dynamics provided a necessary requirement for pattern formation in the stochastic model of  $D_x > 2.48D_y$  whereas the deterministic model provided  $D_x > 27.8D_y$  [10].

The stochastic model can generate Turing patterns where the deterministic model cannot, called quasi-patterns. An explanation may be provided in terms of the fixed points. In our linear stability analysis, the regions where the growth-rate of the  $k = 0$  modes was maximal indicated attraction of the full-non-linear system towards a homogeneous fixed and the Turing instability was formed when the system became attracted to a  $k \neq 0$  fixed-point. However, in actuality, the  $k = 0$  fixed point may be metastable, meaning that sufficiently large fluctuations can push the system out of the basin of attraction and destabilize the homogeneous solution. Giant amplification then plays the role of amplifying the noise to reach instability [11].

Karig et. al. were able to provide evidence for the formation of quasi-patterns by genetically engineering bacterial cells to respond to small molecule inhibitors and activators, *N*-(3-oxododecanoyl) homoserine lactone and *N*-butanoyl-L-homoserine lactone respectively. The activator simultaneously triggered the production a red fluorescent, making the patterns measurable. After about 16 hr, the fluorescent had formed into dots which were determined to be Turing patterns. Deterministic and stochastic modeling of the system confirmed that the diffusion constants of the small-molecule inhibitor was too slow relative to the activator to form normal Turing patterns, indicating that the patterns were likely quasi-patterns [11].

The theoretical and experimental evidence for quasi-patterns in stochastic systems may provide an explanation for why so many pattern form in nature when the conditions for deterministic Turing patterns are so narrow.

## 6 Conclusion

Pattern formation is an emergent phenomena observed throughout nature, where a seemingly homogeneous initial condition evolves towards a, usually steady-state, finite wavelength structure which does not depend on boundary conditions or initial symmetries. Turing's description of a fast-moving inhibitor morphogen and a slow-moving activator in reaction-diffusion systems seems to be a good framework for describing these patterns. However, Turing patterns are not always so easily formed and the conditions for which they can form provide information about the interactions and morphogens which comprise of the system.

In this term essay, we applied linear stability analysis to build a phenomenological picture as to why Turing patterns form and what the conditions for their formation are. We then discussed the implications of said patterns on how asymmetries might form in biological systems, using the hydra as an example. We described two confirmed examples of Turing pattern formation, the chemical CIMA system and the biological

formation of stripes on zebra fish, and the difficulties in ensuring the Turing instability conditions are met. Finally, we introduced the idea of stochastic Turing patterns which provide a framework for potentially broadening the conditions under which Turing patterns form.

## References

- [1] Turing, A. "The Chemical Basis of Morphogenesis." *Bulletin of Mathematical Biology*, vol. 52, no. 1–2, Jan. 1990, pp. 153–97.
- [2] Gierer, A. "Chapter 2 Biological Features and Physical Concepts of Pattern Formation Exemplified By Hydra." *Current Topics in Developmental Biology*, vol. 11, Elsevier, 1977, pp. 17–59.
- [3] Meinhardt, H. "Chapter 6 Almost a Summary: Hydra as a Model Organism." *Models of Biological Pattern Formation*, Academic Press, 1982.
- [4] Castets, V., et al. "Experimental Evidence of a Sustained Standing Turing-Type Nonequilibrium Chemical Pattern." *Physical Review Letters*, vol. 64, no. 24, June 1990, pp. 2953–56.
- [5] De Kepper, P., et al. "Chlorite-Iodide Reaction: A Versatile System for the Study of Nonlinear Dynamic Behavior." *The Journal of Physical Chemistry*, vol. 94, no. 17, Aug. 1990, pp. 6525–36.
- [6] Lengyel, I., and Epstein, I. R. "A Chemical Approach to Designing Turing Patterns in Reaction-Diffusion Systems." *Proceedings of the National Academy of Sciences*, vol. 89, no. 9, May 1992, pp. 3977–79.
- [7] Meinhardt, H., and Gierer, A. "Pattern formation by local self-activation and lateral inhibition." *Bioessays* 22.8, Aug. 2000, pp. 753-760.
- [8] Nakamasu, A., et al. "Interactions between Zebrafish Pigment Cells Responsible for the Generation of Turing Patterns." *Proceedings of the National Academy of Sciences*, vol. 106, no. 21, May 2009, pp. 8429–34.
- [9] Kondo, S., and Miura, T. "Reaction-Diffusion Model as a Framework for Understanding Biological Pattern Formation." *Science*, vol. 329, no. 5999, Sept. 2010, pp. 1616–20.
- [10] Butler, T., and Goldenfeld, N. "Fluctuation-Driven Turing Patterns." *Physical Review E*, vol. 84, no. 1, July 2011, p. 011112.
- [11] Karig, D., et al. "Stochastic Turing Patterns in a Synthetic Bacterial Population." *Proceedings of the National Academy of Sciences*, vol. 115, no. 26, June 2018, pp. 6572–77.